Article

Not peer-reviewed version

From Luminal to Triple Negative: 3D Spheroids Reveal Molecular and Phenotypic Differences Across Breast Cancer Subtypes

Maria Miguel Castro , Leticia Maretti , Catarina Esquível , Bárbara Sousa , Carmen Jerónimo , Andrew J Ewald , Joana Paredes *

Posted Date: 31 March 2026

doi: 10.20944/preprints202603.2418.v1

Keywords: breast cancer; molecular subtypes; 3D tumour spheroids; EMT

 doi:10.20944/preprints202603.2418.v1

Article

From Luminal to Triple Negative: 3D Spheroids Reveal Molecular and Phenotypic Differences Across Breast Cancer Subtypes

Maria Miguel Castro [1,2,3,4,†], Letícia Maretti [1,4,5,†], Catarina Esquível [1,4,5], Bárbara Sousa [1,4], Carmen Jerónimo [3,4,5], Andrew J Ewald [6,7,8] and Joana Paredes [1,2,4,*]

[1] i3S – Institute for Research and Innovation in Health, University of Porto, 4200-135 Porto, Portugal
[2] FMUP – Faculdade de Medicina da Universidade do Porto, Porto, Portugal
[3] Cancer Biology and Epigenetics Group, Research Center of IPO Porto (CI-IPOP) / CI-IPOP@RISE Health Research Network - Portuguese Oncology Institute of Porto (IPO Porto)
[4] Porto Comprehensive Cancer Center Raquel Seruca (P.CCC Raquel Seruca), Porto 4200-072
[5] ICBAS - Instituto de Ciências Biomédicas Abel Salazar, Porto 4050-313, Portugal
[6] Department of Cell Biology, Johns Hopkins University School of Medicine, Baltimore, MD, USA
[7] Giovanis Institute for Translational Cell Biology, Johns Hopkins University School of Medicine, Baltimore, Maryland, United States of America
[8] Cancer Invasion and Metastasis Program, Sidney Kimmel Comprehensive Cancer Center, Johns Hopkins University, Baltimore, Maryland, United States of America
* Correspondence: jparedes@i3s.up.pt
† equally contributing first author.

Abstract

Breast cancer is classified into distinct molecular subtypes, including Luminal A, Luminal B, HER2-enriched, Basal-like, and Claudin-low. While traditional studies mostly use 2D cell cultures, 3D models better mimic *in vivo* tumour conditions. In this study, we generated and characterized 3D spheroids from breast cancer cell lines representing different molecular subtypes. Morphologically, spheroids were either compact (MCF-7/AZ, T47D, BT474, MDA-IBC-3, BT-20, SUM149PT) or loosely adhered (MDA-MB-468, SK-BR-3, MDA-MB-231), while retaining key parental subtype biomarkers. Cell viability decreased with increasing spheroid size, but apoptotic cCasp3 staining was restricted to basal-like spheroids. Compact spheroids expressed E- and/or P-cadherin, indicating epithelial or epithelial–mesenchymal transition (EMT) hybrid traits, while loose spheroids showed vimentin expression linked to a mesenchymal phenotype. In conclusion, EMT-associated features, rather than intrinsic molecular subtype, may contribute to 3D spheroid architecture of breast cancer cell lines.

Keywords: breast cancer; molecular subtypes; 3D tumour spheroids; EMT

1. Introduction

Breast cancer is a significant global health challenge, recognized as the most prevalent malignancy worldwide, accounting for approximately 11.6% of all new cancer diagnoses annually [1], and remains the leading cause of cancer-related mortality among women worldwide. It is a highly heterogeneous disease that comprises several molecular subtypes and varying cellular morphologies, which significantly impact its prognosis and treatment strategies [2]. In the last decades, transcriptomic studies have established five intrinsic breast cancer molecular subtypes: Luminal A, Luminal B, HER2-enriched, basal-like, and claudin-low, each exhibiting distinct underlying biology, prognosis, and clinical behaviour [3–5]. Luminal tumours usually express hormonal receptors (ER and PR) and respond to endocrine therapy, which are further classified into two subtypes: Luminal A and Luminal B. While Luminal A is characterized by high expression of ER and/or PR, lack of HER2

 doi:10.20944/preprints202603.2418.v1

overexpression and low levels of Ki-67, Luminal B exhibits lower hormone receptor expression, may present HER2 positivity, and show higher levels of Ki-67, being correlated with a more aggressive phenotype, therapy resistance and poor prognosis compared to Luminal A [6,7]. Conversely, HER2-enriched breast cancer is characterized by the overexpression of HER2, leading to aggressive tumour growth and metastasis[8,9]; however, HER2-targeted therapies have significantly improved these patients' outcomes [10,11]. Basal-like tumours are predominantly triple-negative (ER, PR, and HER2-negative), displaying high proliferation rates, genetic instability, enrichment of basal mammary markers, and poor prognosis [12,13]. Finally, claudin-low tumours are considered a distinct subtype characterized by low expression of claudins and tight junction cell-cell adhesion proteins, as well as by an enrichment of stem cell-like features, being also predominantly triple-negative breast cancers [14].

Two-dimensional (2D) monolayer culture systems are widely used in cancer research because of their low cost and simplicity. However, these 2D systems do not replicate *in vivo* conditions and the complexity of the tumour microenvironment. *In vivo*, tumour cells grow in a complex three-dimensional (3D) architecture, where gradients of oxygen, nutrients, and metabolites establish heterogeneoecus zones of proliferation, hypoxia, and necrosis [15]. Additionally, dynamic cell–cell and cell-extracellular matrix (ECM) interactions influence key cellular processes, such as cell differentiation, invasion, and drug resistance. These processes are incompletely modelled in 2D systems, which limits their translational relevance [15,16]. Diverse 3D culture systems have been developed, including spheroids, organoids, and scaffold-based models, to provide a more physiologically relevant platform for cancer research. Among them, tumour spheroids represent a robust, reproducible, and cost-effective approach that mimics the structural and functional characteristics of solid tumours [17,18]. Spheroids recapitulate essential features of tumour biology, such as the establishment of proliferation gradients, induction of hypoxia-mediated signalling, altered gene expression profiles, and reduced drug penetration [19]. Larger spheroids, above the critical size of 400-600 μm, sustain oxygen and nutrient gradients. The result is the formation of a central necrotic core, similar to that observed in poorly vascularized tumours, leading to the formation of three different layers of cells: proliferative cells on the outer layer, quiescent cells on the inner layer, and necrotic cells in the spheroids' core [15,18,20]. However, even spheroids between 200-500 μm are sufficiently large to develop gradients of oxygen, nutrients, and catabolites [20,21]. We anticipate that breast cancer cell lines from different molecular subtypes should exhibit distinct capacities to form and maintain 3D spheroids, which would reflect variations in their biology, including the expression of different adhesion molecules, stem-like properties, and metabolic adaptation.

In this study, we generated and characterized tumour spheroids from breast cancer cell lines representing distinct molecular subtypes. By comparing spheroids' morphology, growth kinetics, circularity, and viability, we aimed to identify subtype-specific features that may underlie differences in tumour behaviour and therapy response. A better understanding of these differences may not only enhance the predictive value of 3D preclinical models, but also guide the development of subtype-specific therapeutic strategies.

2. Results

2.1. Establishment and Characterization of Breast Cancer Tumour Spheroids

In vitro 3D breast cancer tumour spheroids were generated, using monocultures of 9 breast cancer cell lines representing distinct molecular subtypes: MCF-7/AZ and T47D as Luminal A; BT474 as Luminal B; SK-BR-3 and MDA-IBC-3 as HER2-enriched; BT-20 and MDA-MB-468 as Basal-like; and MDA-MB-231 and SUM149PT as Claudin-low (Table 1). These molecular subtypes were determined based on previous studies performed by Neve et al [22] and Prat A et al [14]. To establish these spheroids, microwell array technology was used as previously described [23,24] (Figure A1). Briefly, cells were seeded in different numbers (1000, 2500, and 5000 cells per spheroid) into agarose

 doi:10.20944/preprints202603.2418.v1

micro-molds, where cell-surface interactions are minimized, due to non-adhesive and hydrophilic properties, leading to spheroid formation due to cell-cell adhesion cues.

Table 1: Breast cancer cell lines used in this study, with their clinical origin, source and molecular tumour features

				Molecular subtype	
Cell line	**Disease**	**Source**	**Molecular markers**	Neve *et al*[&]	Prat A *et al*[#*]
MCF-7/AZ	Invasive breast carcinoma	Pleural Effusion	ER+/PR+/HER2-	Luminal	Luminal
T47D	Invasive breast carcinoma	Pleural Effusion	ER+/PR+/HER2-		
BT474	Invasive breast carcinoma	Primary tumour	ER+/PR+/HER2+		HER2-enriched
SK-BR-3	Breast adenocarcinoma	Pleural effusion	ER-/PR-/HER2+		HER2-enriched
MDA-IBC-3	Breast inflammatory carcinoma	Pleural effusion	ER-/PR-/HER2+	-	HER2-enriched
BT20	Invasive breast carcinoma	Primary tumour	ER-/PR-/HER2-	Basal A	Basal
MDA-MB-468	Breast adenocarcinoma	Pleural effusion	ER-/PR-/HER2-	Basal A	Basal
SUM149PT	Breast inflammatory carcinoma	Primary tumour	ER-/PR-/HER2-	Basal B	Basal/Claudin-low
MDA-MB-231	Breast adenocarcinoma	Pleural effusion	ER-/PR-/HER2-	Basal B	Claudin-low

				Molecular subtype	
Cell line	**Disease**	**Source**	**Molecular markers**	Neve *et al*[&]	Prat A *et al*[#*]
MCF-7/AZ	Invasive breast carcinoma	Pleural Effusion	ER+/PR+/HER2-	Luminal	Luminal
T47D	Invasive breast carcinoma	Pleural Effusion	ER+/PR+/HER2-		
BT474	Invasive breast carcinoma	Primary tumour	ER+/PR+/HER2+		HER2-enriched
SK-BR-3	Breast adenocarcinoma	Pleural effusion	ER-/PR-/HER2+		HER2-enriched
MDA-IBC-3	Breast inflammatory carcinoma	Pleural effusion	ER-/PR-/HER2+	-	HER2-enriched
BT20	Invasive breast carcinoma	Primary tumour	ER-/PR-/HER2-	Basal A	Basal
MDA-MB-468	Breast adenocarcinoma	Pleural effusion	ER-/PR-/HER2-	Basal A	Basal
SUM149PT	Breast inflammatory carcinoma	Primary tumour	ER-/PR-/HER2-	Basal B	Basal/Claudin-low
MDA-MB-231	Breast adenocarcinoma	Pleural effusion	ER-/PR-/HER2-	Basal B	Claudin-low

[&]Neve et al. Cancer Cell, 2006 DOI: 10.1016/j.ccr.2006.10.008; [#]Prat et al. Breast Cancer Research, 2010 DOI: 10.1186/bcr263510; *Prat, et al. Breast Cancer Res Treat, 2013 DOI: 10.1007/s10549-013-2743-3.

 doi:10.20944/preprints202603.2418.v1

2.2. Morphological Characterization of Breast Cancer Tumour Spheroids

Brightfield images were acquired and spheroids' size and circularity (with 1.0 representing a perfect circle) were assessed. Morphological integrity was also evaluated by H&E staining. After 48 hours in culture, distinct patterns of spheroids morphology were observed across the different cell lines tested. A compact and well-adherent spheroid was found for MCF-7/AZ, T47D, BT474, MDA-IBC-3, BT-20, and SUM149PT cell lines (Figure 1A). The spheroids' size increased in a cell number-dependent manner and consistently presented high circularity values (approximately 1.0), indicative of their compact and circular morphology regardless of the initial cell number (Figure 1B -1G). Additionally, H&E staining reinforced these observations, showing highly cohesive and compact cellular aggregates formed by these cell lines (Figure A2). It is noteworthy that, for MDA-IBC-3 cell line, spheroids generated with 2500 cells presented a significant higher circularity compared to the ones formed with 1000 cells per spheroid (Figure 1E), while in SUM149PT, 5000 cells/spheroid showed increased circularity compared with 2500 cells/spheroid (Figure 1G).

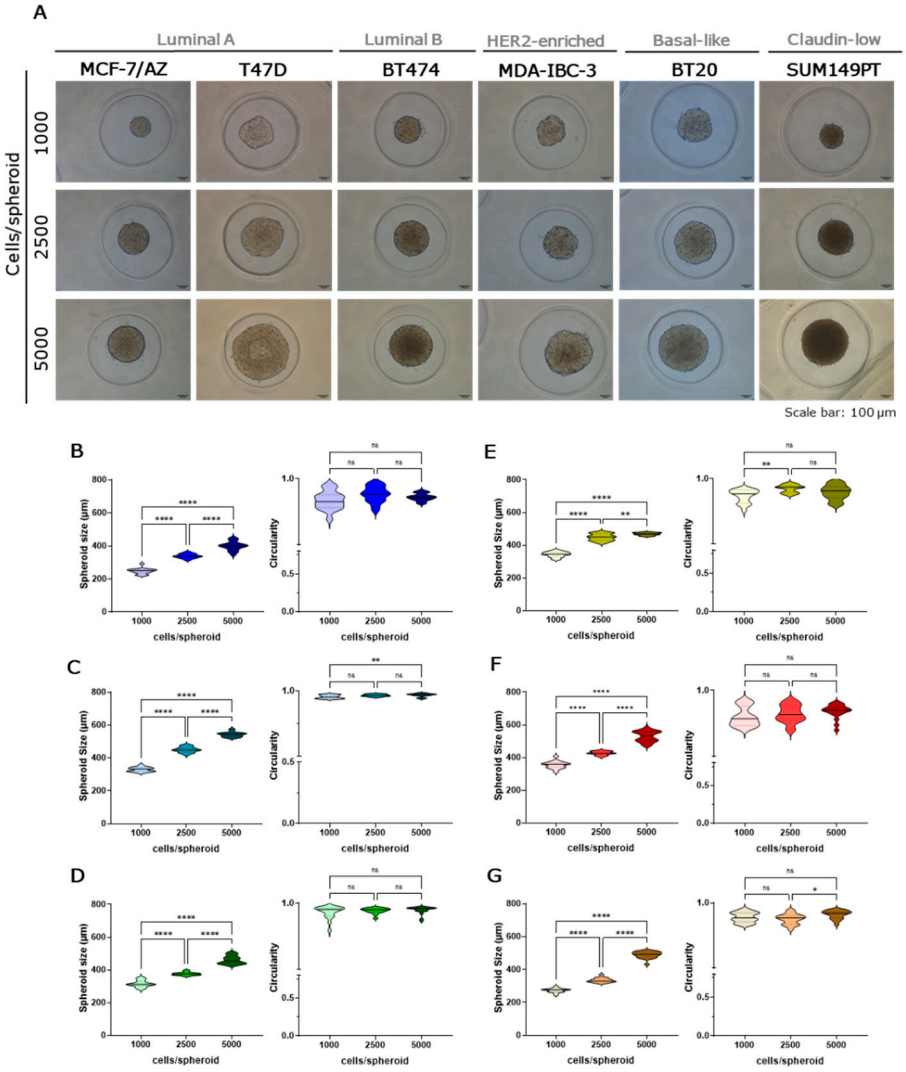

Figure 1. Compact spheroids generated by several breast cancer cell lines [MCF-7/AZ (blue), T47D (blue), BT474 (green), MDA-IBC-3 (yellow/green), BT20 (red) and SUM149PT (brown)] and seeded at three different cell densities (1000, 2500 and 5000 cells/spheroid). Brightfield microscopy images of spheroids' morphology after 48h. Scale bars represent 100 µm [A]. Measurement of spheroids' size and circularity for MCF-7/AZ [B], T47D [C], BT474 [D], MDA-IBC-3 [E], BT20 [F], and SUM149PT [1G] using the Harmony high-content imaging and analysis software in three independent experiments. Data are shown as mean ± SD and the level of significance was set at *p<0.05, **p<0.01, ***p<0.001 and ****p<0.0001.

 doi:10.20944/preprints202603.2418.v1

Conversely, loosely adhered spheroids were found with SK-BR-3, MDA-MB-468, and MDA-MB-231 cell lines (Figure 2A). These spheroids showed lower circularity and size variability across seeding densities. Regarding spheroids' size, for the SK-BR3 cell line, the ones formed with 2500 cells were significantly larger than those formed with both 1000 and 5000 cells (Figure 2B). But, as expected, 5000 cells generated significantly larger spheroids than 1000 cells. In MDA-MB-468 cell line, spheroids' size increased with seeding density; however, no statistically significant differences were observed between 2500 and 5000 cells per spheroid (Figure 2C). Less cohesive and circular aggregates were also confirmed by H&E staining, which also indicated no evidence of necrotic core in any spheroid across all tested seeding densities (Figure A2).

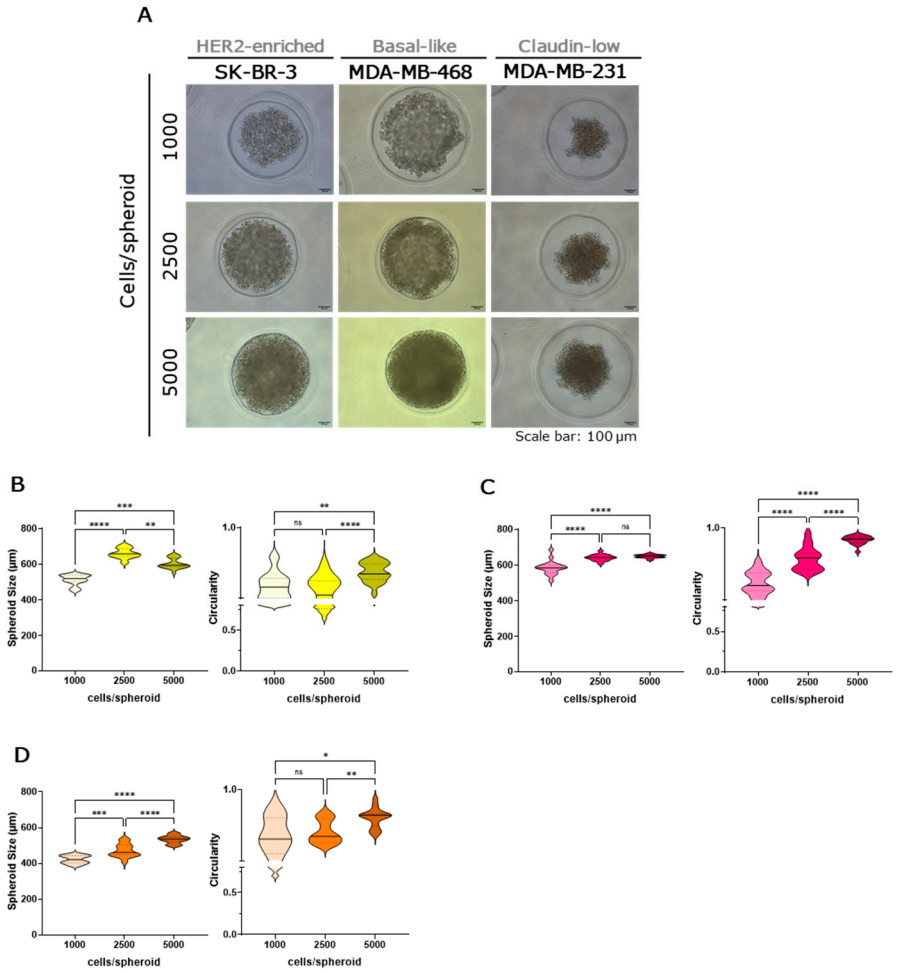

Figure 2. Loosely adhered spheroids generated by several breast cancer cell lines [SK-BR-3 (yellow), MDA-MB-468 (pink), and MDA-MB-231(orange)] and seeded in three different cell densities (1000, 2500 and 5000 cells/spheroid). Brightfield microscopy images of spheroids' morphology after 48h. Scale bars represent 100 µm [A]. Measurement of spheroids size and circularity for SKBR-3 [B], MDA-MB-468 [C] and MDA-MB-231 [D] using the Harmony high-content imaging and analysis software in three independent experiments. Data are shown as mean ± SD and the level of significance was set at *p<0.05, **p<0.01, ***p<0.001 and ****p<0.0001.

2.3. Molecular Characterization of Breast Cancer Tumour Spheroids

Breast cancer molecular subtypes were validated qualitatively by immunohistochemistry, using key markers such as ER, PR, HER2, and Ki-67 (Figure 3 and A3). As expected, Luminal A (MCF-7/AZ and T47D) spheroids were positive for both ER and PR. However, although MCF-7/AZ showed negativity for HER2, as expected, T47D spheroids showed HER2 positivity. Regarding Ki-67, MCF-7/AZ spheroids presented high expression for this marker, while the T47D ones showed lower levels; however, both demonstrated widespread nuclear staining throughout the spheroid core. For Luminal

 doi:10.20944/preprints202603.2418.v1

B (BT474) spheroids, a strong HER2 expression was found, as well as positivity for both ER and PR. An intermediate Ki-67 staining was observed, with a slightly more heterogeneous distribution. Concerning SK-BR-3 and MDA-IBC-3, both presented strong HER2 expression, as expected, and were negative for ER and PR. High Ki-67 expression was observed in SK-BR-3, whereas MDA-IBC-3 showed lower expression levels of this marker. In both cell lines, positive nuclei were dispersed throughout spheroid structures. As expected, spheroids derived from the basal-like (BT-20 and MDA-MB-468) and claudin-low (SUM149PT and MDA-MB-231) molecular subtypes were triple-negative for classical receptors (ER-, PR-, and HER2-). For Ki-67, high expression was observed in BT-20 and MDA-MB-468 spheroids, consistent with their known aggressive and fast-growing phenotype. Claudin-low spheroids displayed a lower proliferation index. MDA-MB-231 showed low and sparse Ki-67-positive nuclei, while SUM149PT presented an intermediate expression, mainly localized in spheroids' core.

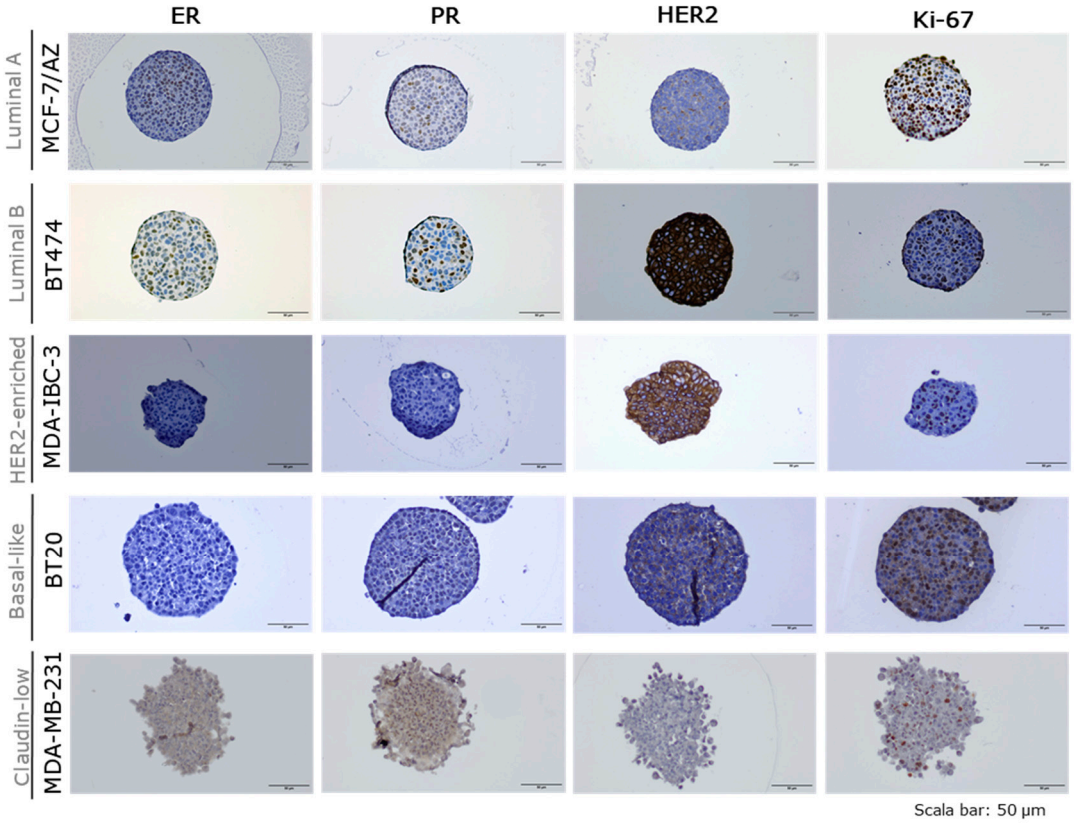

Figure 3. Representative images of each breast cancer molecular subtype (Luminal A- MCF-7/AZ; Luminal B-BT474; HER2-enriched–MDA-IBC-3; Basal-like-BT20; and Claudin-low–MDA-MB-231). Immunohistochemistry for Hormonal receptors (ER-Estrogen; PR-Progesterone), human epidermal growth factor receptor 2 (HER-2) and Ki67 (proliferation marker) using breast cancer spheroids (2500 cells/spheroid). Scale bars represent 50 µm.

2.4. Viability and Cell Death in Breast Cancer Tumour Spheroids

Cell viability was evaluated through a live/dead staining, using Calcein-AM and propidium iodide (PI) staining after 48 hours in suspension (Figure 4 and A4). SK-BR-3, MDA-IBC-3, MDA-MB-231, MDA-MB-468, and SUM149PT spheroids showed a statistically significant decrease in viability in a cell-number-dependent manner. Conversely, MCF-7/AZ spheroids, formed with 1000 cells, presented the lowest viability compared to 2500 and 5000 cells per spheroid. 5000 cells per spheroid of T47D, BT474, and BT-20 showed the lowest viability; however, no statistically significant differences were observed between 1000 and 2500 cells per spheroid. In addition, cell death mechanisms were assessed using immunofluorescence staining for cCasp3, a well-established marker

 doi:10.20944/preprints202603.2418.v1

of apoptosis. Basal-like spheroids were the only ones exhibiting positive expression, mainly in the core, which suggests central apoptotic activity.

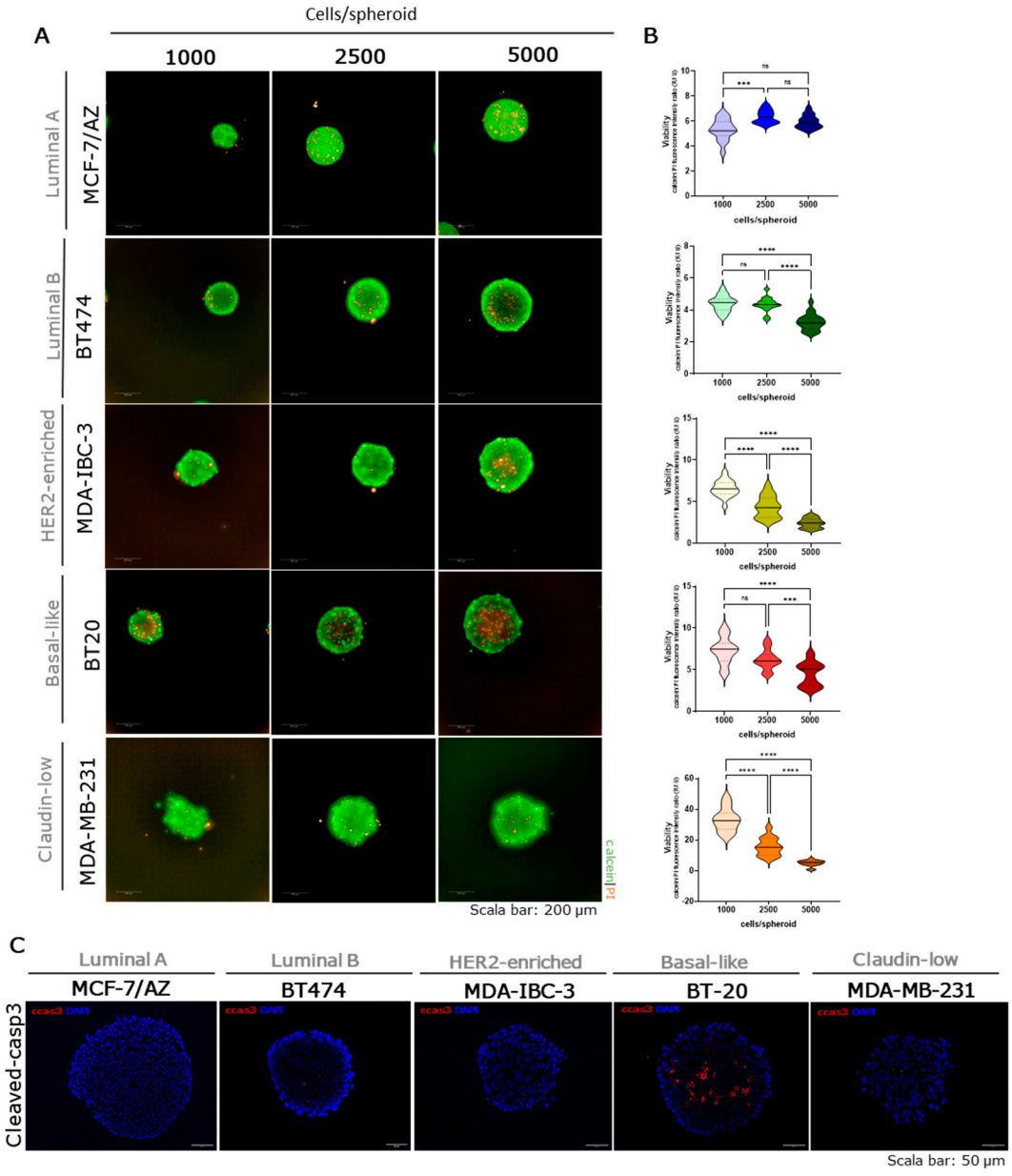

Figure 4. Evaluation of cell viability and cleaved-caspase 3 for each breast cancer molecular subtype: Luminal A-MCF-7/AZ (blue); Luminal B-BT474 (green); HER2-enriched–MDA-IBC-3 (yellow/green); Basal-like-BT20 (red); and Claudin-low–MDA-MB-231(orange). Viability was evaluated using calcein/PI staining, where calcein (green) label live cells, and PI (red) the dead cells. Scale bars represent 200 µm [A]. Quantification of the fluorescent intensity (RFU -relative fluorescent units) of calcein and PI ratio using the Harmony high-content imaging and analysis software in three independent experiments [B]. Representative images of cleaved-caspase-3 (cCasp3, red) staining and nuclei counterstained with DAPI (blue) in the 2500 cells/spheroid after 48h in suspension. Scale bars represent 50 µm [C]. Data are shown as mean ± SD, and the level of significance was set at *p<0.05, **p<0.01, ***p<0.001 and ****p<0.0001.

2.5. Epithelial-Mesenchymal Transition in Breast Cancer Tumour Spheroids

Epithelial-mesenchymal transition (EMT) is a biological process characterized by the conversion of epithelial cells into more invasive mesenchymal cells. This transition involves a complex reprogramming of gene expression, leading to the downregulation of epithelial markers, such as E-

 doi:10.20944/preprints202603.2418.v1

cadherin, and the upregulation of mesenchymal markers, including vimentin [25,26]. The co-expression of E- and P-cadherin has been established as a possible marker of a hybrid EMT phenotype [25,27–30]. Spheroids' epithelial and mesenchymal phenotypes were qualitatively assessed using immunofluorescence staining of epithelial (E-cadherin), mesenchymal (vimentin), and hybrid (E- and P-cadherin) markers. (Figure 5 and A5).

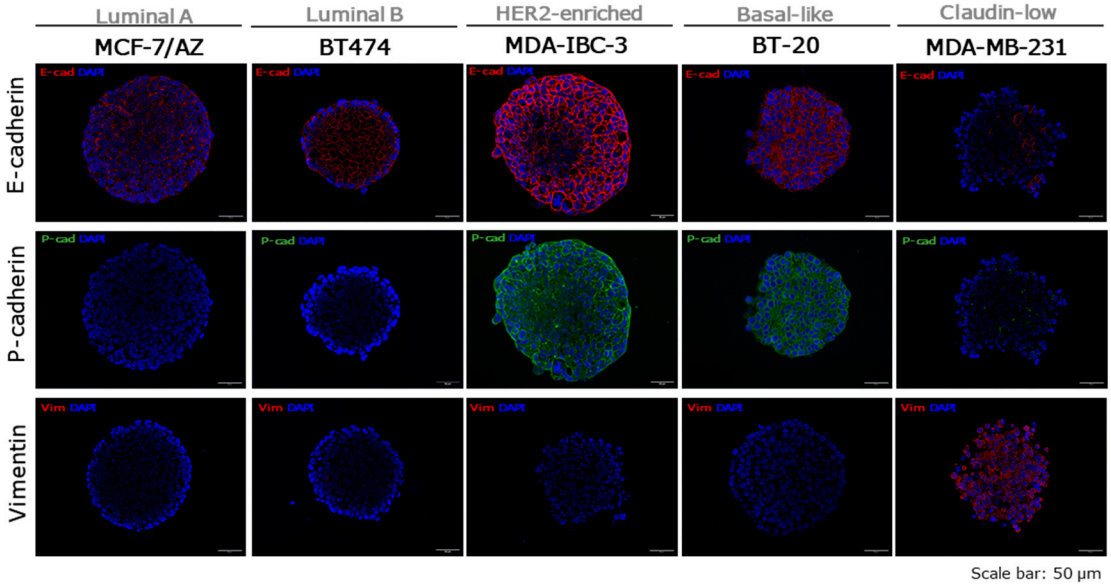

Figure 5. Representative images showing the expression of EMT markers for each breast cancer molecular subtype (Luminal A- MCF-7/AZ; Luminal B-BT474; HER2-enriched–MDA-IBC-3; Basal-like-BT20; and Claudin-low–MDA-MB-231). E-cadherin staining (red) was used as an epithelial marker, Vimentin staining (red) as a mesenchymal marker, and E-cadherin (red) and P-cadherin (green) representing the hybrid EMT phenotype. All samples were counterstained with DAPI (blue). Scale bars represent 50 µm.

The results showed that spheroids representing the Luminal subtype (MCF-7/AZ, T47D, and BT474) exhibited strong membrane expression of E-cadherin and no expression of P-cadherin and vimentin, supporting the epithelial phenotype, as well as the strong compactness and cell-cell adhesion observed before. HER2-enriched SKBR3 spheroids showed vimentin expression at the membrane, but absence of both E- and P-cadherin, indicating a mesenchymal phenotype consistent with their loose adhesion. In contrast, MDA-IBC-3 spheroids revealed strong co-expression of both cadherins at the cell membrane, with no vimentin expression, demonstrating an epithelial phenotype and consistent adhesive behaviour. Basal-like spheroids (MDA-MB-468 and BT-20) showed co-expression of both E- and P-cadherin. While no vimentin expression was observed in BT-20 spheroids, MDA-MB-468 spheroids showed slight vimentin expression. This result is consistent with the strong compactness of BT-20 spheroids, but also with the loose aggregation of MDA-MB-468 spheroids. In the claudin-low subtype, MDA-MB-231 spheroids showed minimal E- and P-cadherin expression and strong vimentin expression, in accordance with their loose adhesion profile. Conversely, SUM149PT spheroids, similarly to MDA-IBC-3, showed a strong E- and P-cadherin co-expression and no vimentin, indicating a hybrid EMT phenotype consistent with the cell-cell adhesion observed during spheroid formation. Supporting these observations, we performed a bioinformatic analysis using data from the Cancer Cell Line Encyclopedia (CCLE) to associate the observed 3D spheroid morphology with EMT scores obtained from the Molecular Signatures Database (MSigDB). The analysis indicated that cell lines forming loosely adherent spheroids tend to display higher EMT scores, consistent with a more mesenchymal phenotype, whereas cell lines forming compact spheroids show lower EMT scores, indicative of a more epithelial profile. Although this difference did not reach statistical significance, likely due to the limited number of cell lines analysed, the results support our observation that epithelial-like cell lines preferentially form

 doi:10.20944/preprints202603.2418.v1

compact spheroids, while mesenchymal-like cell lines are associated with loosely adherent spheroid structures (Figure A6).

3. Discussion

Over the course of recent years, 3D models have become widely applied in cancer research, providing a valuable tool to evaluate drug response, tumour-specific growth patterns, and cell-cell interactions. These models provide a more physiologically relevant system for cancer research by more accurately mimicking in vivo architecture and tumour microenvironment than 2D models [15]. In this study, we successfully established and characterized 3D breast cancer tumour spheroids across nine cell lines representing distinct molecular subtypes.

Morphological analyses revealed differences in spheroid integrity and cohesion. Luminal A and B cell lines (MCF-7/AZ, T47D, BT474), as well as MDA-IBC-3, BT-20, and SUM149PT, formed compact, highly circular spheroids, reflecting strong cell-cell adhesion and enriched epithelial characteristics. Actually, T47D spheroids showed a lumen formation, which is a distinctive morphological feature that has been previously reported in the literature under different cell densities and incubation times [31,32]. In contrast, SK-BR-3, MDA-MB-468, and MDA-MB-231 produced loosely aggregated, irregular spheroids, indicative of a weaker cohesion and more mesenchymal-like traits. Our results are in accordance with the literature, which shows that SK-BR-3 and MDA-MB-468 presented a grape-like colony morphology in 3D cultures, while MDA-MB-231 displays a stellate structure [33]. Although MDA-MB-468 spheroids exhibited an increase in circularity (approaching 1.0) at the 5000 cells per spheroid condition, this does not reflect the formation of a truly compact spheroid, but rather a technical limitation of the micro-mold culture system. Agarose micro-molds are designed to support spheroid growth within a diameter range of approximately 300–800 μm. Under these conditions, however, MDA-MB-468 spheroids exceeded ~600 μm and approached the physical limits of the microwells. As a result, spatial confinement likely restricted normal spheroid expansion, and mechanical constraints imposed by the well walls artificially increased the measured circularity. Additionally, another study established that SK-BR-3 and MDA-MB-231 cells presented loose aggregates or single-cell suspension structures for spheroids generated using the liquid overlay technique [34]. The morphological differences observed were partly dependent on initial seeding density, with higher cell numbers generally promoting larger spheroids [24,35,36], although some cell lines displayed non-linear growth patterns, suggesting intrinsic regulation of cell-cell adhesion and proliferation. H&E staining corroborated these observations, highlighting cohesive cellular architecture in compact spheroids and loose organization in mesenchymal-like spheroids, with no necrotic cores observed across the 48 hours culture period. One of the limitations of our study is the suspension period, since the extension of the culture period may alter these results, leading to increased necrosis in the spheroid core. Additionally, a cell organization and ultrastructure study could be performed to better understand the differences in spheroids over time of incubation.

Molecular characterization confirmed that 3D spheroids retained the key markers of their parental molecular subtypes [37–40]. Luminal spheroids were positive for ER and PR, with variable Ki-67 proliferation patterns; notably, MCF-7/AZ exhibited widespread high Ki-67 expression, which contrasts with prior reports showing low proliferative capacity of MCF-7 cells in 3D spheroids [41,42]. It is important to consider that in one of the studies the spheroids were performed in a scaffold-based method in collagen type I [41], and that in the other study, they used different cell line media [42], which can have an impact on the expression of biological markers [43]. T47D showed some Ki-67 peripheral localization, suggesting potential gradients in proliferation even in the absence of necrosis. Additionally, T47D showed HER2 expression in 3D spheroids, even though this cell line has already been described as HER2 negative in 2D cultures. However, one study shows that T47D long-term treated with an anti-estrogen drug can resist and shift from ER+/HER2- to HER2+/Src+, with a significant increase of HER2 expression and Src activity [44]. Moreover, an increase in fibronectin was already found in MDA-MB-231, which increases the activity of Src [45], and it was already reported that T47D 3D models show an increase in fibronectin mRNA levels expression [46]. Thus, our data

 doi:10.20944/preprints202603.2418.v1

suggest the hypothesis that T47D grown in 3D can have more fibronectin and adhesion molecules expression, like FAK, which can increase Src activation and consequently the HER2 activation in spheroids. However, this hypothesis requires additional validation, since we only assessed qualitatively. HER2-enriched spheroids demonstrated expected HER2 expression, but varied in proliferation, with SK-BR-3 showing high Ki-67 and MDA-IBC-3 exhibiting lower, more heterogeneous proliferation, highlighting intra-subtype heterogeneity. Basal-like and claudin-low spheroids maintained their triple-negative status, with basal-like cell lines showing high Ki-67 and central apoptosis, consistent with aggressive, rapidly proliferating phenotypes [47]. Claudin-low spheroids, particularly MDA-MB-231, displayed lower proliferation rates, reflecting the mesenchymal/stem-like phenotype characteristic of this subtype [14], where cells exhibit increased invasive capacity, rather than proliferative competence.

Cell viability analyses further emphasized molecular subtype-dependent behaviours. Viability decreased with increasing spheroid size in several cell lines, particularly in SK-BR-3, MDA-IBC-3, MDA-MB-231, MDA-MB-468, and SUM149PT, suggesting limitations in nutrient diffusion or accumulation of apoptotic signals [24,35,36].

Overall, the viability results indicate that compact spheroids exhibit increased cell death in the core and lower overall viability compared to loosely adherent spheroids, in which dead cells are more dispersed throughout the structure rather than concentrated in the center. Previous studies suggest that compact spheroids consume oxygen at a higher rate than loosely adherent ones and develop steeper hypoxic gradients from the surface to the core, indicating that oxygen distribution is closely related to spheroid compactness [48]. Additionally, Zanoni *et al.* reported that variations in spheroid shape (spherical versus non-spherical) can influence cell viability. The authors hypothesized that non-spherical spheroids may contain a greater proportion of viable cells because the reduced distance between individual cells and the culture medium interface increases the area available for active proliferation [49]. However, in the MCF-7/AZ cell line, cell viability did not decrease in the largest spheroids, unlike what was observed for the other cell lines. One possible explanation is that the size of these spheroids remained below 400 μm. According to the literature, oxygen and nutrient diffusion are more efficient in smaller spheroids, preventing the formation of severe hypoxic or necrotic regions [15,20]. Furthermore, previous studies have shown that 48 hours in 3D culture may be insufficient to significantly reduce cell viability in MCF-7 spheroids generated using different 3D culture systems [50,51]. Therefore, it is possible that longer culture periods would lead to the development of a necrotic core in these spheroids, similar to what has been reported for other cell lines under comparable conditions. cCasp3 expression was restricted to basal-like spheroids, mainly in the core, indicating central apoptosis as a feature of this aggressive molecular subtype [52]. Qualitative assessment of EMT markers revealed a strong correlation between EMT phenotype and spheroid morphology [37,45], although with notable exceptions. Luminal spheroids expressed E-cadherin and lacked P-cadherin and vimentin, consistent with their epithelial phenotype and compact morphology. SK-BR-3 and MDA-MB-231 spheroids presented a mesenchymal phenotype (vimentin positive), aligning with their loose adhesion, whereas MDA-IBC-3 and SUM149PT exhibited a hybrid EMT phenotype, with co-expression of E- and P-cadherin, yet retaining compact morphology, suggesting that partial EMT states may support both cell-cell adhesion and invasive potential [28]. Basal-like cell lines (BT-20 and MDA-MB-468) also showed E- and P-cadherin co-expression, but morphological outcomes varied, implying additional factors contributing to spheroid cohesion. Notably, it has been demonstrated that α-catenin exons 4 and 5 are homozygously deleted from the genome of MDA-MB-468 cells, leading to two aberrant transcript lengths, which contribute to their loose aggregation and vimentin expression, besides cadherins expression [53]. Overall, EMT-associated features, rather than molecular subtype, seem to contribute to spheroid's morphology, with the mesenchymal phenotype (vimentin-positive) exhibiting loosely aggregated spheroids, and the epithelial-hybrid phenotype (E-cadherin and P-cadherin positive) characterized by a more compact organization.

 doi:10.20944/preprints202603.2418.v1

In brief, our findings highlight the capacity of 3D spheroid models to recapitulate the intrinsic heterogeneity of breast cancer subtypes, encompassing differences in morphology, proliferation, EMT status, and viability. Although numerous studies already exist in the literature employing breast cancer spheroids, most of them only use one or two cell lines [33,34,54–56], involve co-cultures with stromal or immune cells [57–61], test for drugs response [36,62,63], and do not employ the specific agarose micro-mold culture model used in this study. This work's novelty lies in the extensive characterization of nine breast cancer cell lines across different molecular subtypes and their correlation with the EMT status and spheroids' morphology. Moreover, it provides a new, reliable platform for generating 3D spheroids using agarose micro-molds, providing a robust basis for studying subtype-specific biology, including responses to therapies, EMT processes, and cell-cell interactions. One of the major advantages of this model is the possibility of doing co-cultures with several types of cells, such as immune, stromal, and/or endothelial cells [23,24,64,65]. Future studies should explore longer-term cultures to assess necrotic core formation and integrate stromal or immune components to better mimic the tumour microenvironment. Additionally, investigating the mechanisms underlying discrepancies between EMT markers expression and spheroids morphology could yield insights into cell-cell adhesion, invasiveness, and metastatic potential. Overall, while cell line–derived 3D spheroids lack stromal and immune components and are cultured in serum-supplemented media, they provide a reproducible and standardized platform for comparative analyses across breast cancer models before validation in more complex systems, such as patient-derived organoids or co-culture models.

4. Materials and Methods

4.1. Breast Cancer Cell Lines

Breast cancer cell lines were obtained as follows: MCF-7/AZ, from Prof. Marc Mareel's lab (Ghent University, Belgium); T47D, BT474, SK-BR-3, MDA-MB-231, BT-20, and MDA-MB-468, from ATCC (Manassas, VA, USA); MDA-IBC-3, kindly provided by Prof. Wendy Woodward; and SUM149PT, kindly supplied by Dr. Stephen Ethier. MCF-7/AZ was cultured in DMEM/F12 (Invitrogen Ltd, UK), and T47D was cultured in RPMI 1640 with GlutaMAX (Gibco, Thermo Fisher Scientific, USA). Both media were supplemented with 10% FBS (Cythiva, USA) and 1% Pen-Strep (Invitrogen Ltd, UK). BT474 was cultured in DMEM/F12 supplemented with 10% FBS, 2 mM L-Glutamine (Sigma Aldrich, USA), 5 µg/mL Insulin (Sigma-Aldrich, USA), and 1% Pen-Strep. SK-BR-3, MDA-MB-231, BT-20, and MDA-MB-468 were cultured on DMEM with 10% FBS and 1% Pen-Strep. MDA-IBC-3 was cultured in Ham's F12, with 10% FBS, 1 µL/mL Hydrocortisone (Sigma Aldrich, USA), 5 µg/mL Insulin, 1% Pen-Strep, and 1 M HEPES (Sigma Aldrich, USA). SUM149PT was cultured on DMEM/F12 with 5% FBS, 1 µg/mL Hydrocortisone, 5 µg/mL Insulin, and 1% Pen-Strep. All cell lines were maintained at 37°C in a humidified atmosphere containing 5% CO_2.

4.2. Breast Cancer Tumour Spheroids

Breast cancer tumour spheroids were generated through the liquid overlay technique using commercially available micro-molds (3D Petri Dish®, from Micro Tissues Inc.) (Figure A1) [23,24]. First, 2% (w/v) agarose (Grisp Research Solutions, Portugal) was dissolved in 0.9% (w/v) NaCl (Merck, Germany) and cast in 3D Petri Dish micro-molds to form agarose molds with 81 uniform circular microwells. Then, molds were placed in a 12-well plate and incubated with cell culture media (190 µl to the molds and 1mL to the wells) to equilibrate the molds for at least 2 hours. Afterwards, cells were collected and counted to prepare an adequate cell suspension, according to the three different total numbers of cells per spheroid tested (1000, 2500, and 5000 cells per spheroid). Finally, the medium was removed, and the cell suspension (190 µl) from each breast cancer cell line was added to the mold and incubated for 30 minutes. Finally, cell culture medium (2 mL) was added to each well.

 doi:10.20944/preprints202603.2418.v1

4.3. Breast Cancer Spheroids' Size Measurement

Brightfield images were acquired using a DMi1 inverted microscope (Leica) at 48 hours post-seeding. At the same time point, additional images were acquired using the Operetta CLS High-content Imaging System (Revivity, PerkinElmer, USA), and spheroids' size and circularity were determined using the Harmony-High-Content Imaging and Analysis Software (Revivity, PerkinElmer, USA).

4.4. Breast Cancer Spheroids' Histological Analysis

After 48 hours of incubation time, culture media were gently removed from the wells, and molds were washed twice with PBS. Spheroids were then fixed with 4% (v/v) of formaldehyde for 20 minutes at RT. Then, the formaldehyde was removed, and two more washing steps with PBS were performed. After, 1.5% agarose (w/v) solution was added to the top of each mold and allowed to solidify. Later, molds were embedded in paraffin using an automated embedding system (Thermo Scientific STP 120 Spin Tissue Processor). Paraffin-embedded samples were sectioned into 4 μm sections, deparaffinized in xylene, and rehydrated through a graded alcohol series. H&E staining was performed to assess spheroid morphology. Images were acquired using the Brightfield Microscope Leica DM2000 LED (Leica Microsystems, Germany)

4.5. Breast Cancer Spheroids' Immunohistochemistry

Immunohistochemistry staining was carried out after 48 hours of culture in conditions of 2500 cells/spheroid. Initially, samples were fixed in accordance with the protocol described above, followed by sectioning, deparaffinization in Clear-Rite, and rehydration through a grade series of decreasing ethanol concentrations. Thereafter, antigen retrieval was performed by incubating the sections with the appropriate antigen retrieval buffer – either sodium citrate (pH=6) (Invitrogen, Thermo Fisher Scientific, USA) or Tris/EDTA (pH=9) (Novocastra, Leica Biosystems, UK) - for 30 minutes at 96ºC. After this incubation period, sections were washed twice with PBS for 5 minutes under gentle agitation. Endogenous peroxidase activity was blocked using 3% hydrogen peroxide (Sigma-Aldrich, USA) in 100% methanol (Fisher Scientific, UK), and the sections were again washed twice with PBS. Primary antibodies were used at the dilutions presented in the supplementary Table A1 to evaluate the expression of ER, PR, HER2 and Ki-67. Primary antibody suspension was added to each section and incubated overnight at 4°C in a humidified chamber. Subsequently, samples were washed twice with PBS under the conditions described above. To detect the primary antibody, sections were incubated in HRP polymer (Dako, Agilent Technologies, USA) for 30 minutes. After three washes with PBS, 100μL of DAB reagent (Dako, Agilent Technologies, USA) per mold was added to each section for 5 minutes to visualize the antibody staining. The sections were washed under running tap water twice, for 3 minutes each. Counterstaining was performed by immersing the sections in hematoxylin (Epredia, USA) for 30 seconds to 2 minutes, followed by rinsing under running tap water for 5 minutes. Finally, tissues were dehydrated in three increasing concentrations of alcohol (70%, 100%, and 100%), each for 5 minutes, and cleared with Clear Rite twice for 10 minutes each. Slides were mounted with coverslips using a mounting solution (Richard-Allan Scientific, Thermo Fisher Scientific, USA). Images were acquired using the Brightfield Microscope Leica DM2000 LED (Leica Microsystems, Germany).

4.6. Cell Viability

A fluorescent-based staining protocol was employed, using Calcein-AM, PI, and Hoechst 3342, to assess cell viability within spheroids. Staining solutions were prepared according to Kessel et al. 2017 [66], using the following final concentrations: calcein (1 μM, Invitrogen, Thermo Fisher Scientific, C1430), PI (4 μg/mL, Invitrogen, Thermo Fisher Scientific, P1304MP), and Hoechst (10 mg/mL, Invitrogen, Thermo Fisher Scientific, H3570). After 48 hours, spheroids were washed twice with PBS, and 200 μL of the staining solution was added to each well. The plate was incubated at

 doi:10.20944/preprints202603.2418.v1

room temperature for 45 minutes with gentle agitation (60 rpm). Following the incubation period, spheroids were washed again with PBS, and 200 µL of fresh PBS was added to each well. Images were acquired using the Operetta CLS high-content imaging system (Revvity). The fluorescence signals corresponded to live (green), dead (red), and total (blue) cell populations. Fluorescence intensities of calcein and PI were quantified using the Harmony-High-Content Imaging and Analysis Software (Revivity, PerkinElmer, USA). The software also calculated the calcein/PI fluorescence intensity ratio, which was used as an indicator of cell viability.

4.7. Immunofluorescence

Immunofluorescence staining was carried out after 48 hours of culture in 2500 cells/spheroid for the EMT and cell death biomarkers: E-cadherin, P-cadherin, vimentin, and cleaved-Caspase 3 (cCasp3). First, sections were deparaffinized in Clear-Rite, followed by rehydration through a series of decreasing ethanol concentrations. Thereafter, antigen retrieval was performed as described above. Subsequently, samples were washed twice with PBS for 5 minutes each under gentle agitation (60 rpm). To block non-specific binding, sections were incubated with 5% (v/v) BSA (NZyTech, Portugal) for 30 minutes. Primary antibodies, at the dilutions specified in supplementary Table A1, were then applied and incubated overnight at 4°C in a humidified chamber. Following this, sections were washed three times with PBS and incubated for 1 hour in the dark with the appropriate secondary antibodies diluted 1:500 in BSA: Alexa Fluor 488 Goat Anti-Mouse IgG and Alexa Fluor 594 Goat Anti-Rabbit IgG (Thermo Fisher Scientific). After three additional washes with PBS, sections were mounted using Vectashield containing DAPI (5 µL/section; Vector Laboratories) and imaged with a Zeiss Axio Imager fluorescence microscope (Carl Zeiss AG, Germany).

4.8. Bioinformatics Analysis

4.8.1. CCLE Dataset

Normalized gene expression data for the expression of 53,971 genes in different breast cancer cell lines was retrieved from the Cancer Cell Line Encyclopedia (CCLE, https://depmap.org/portal/ [accessed on 11 March 2026]). Only the data from the cell lines of interest for this study (BT474, MCF-7/AZ, T47D, BT-20, MDA-MB-468, MDA-MB-231, SK-BR3, SUM149PT) were used for analysis; data from MDA-IBC3 was not available. Cell line annotations, including DepMap IDs and stripped cell line names were obtained from the CCLE cell line metadata file (sample_info.csv). The dataset was filtered to include only breast cancer lines with complete expression and annotation data. Expression values were log2-transformed RNA-seq TPM levels, as provided by CCLE.

4.8.2. EMT Gene Selection

Hallmark Epithelial-Mesenchymal Transition (EMT) genes were retrieved from the Molecular Signatures Database using the msigdbr R package. A total of 200 genes associated with EMT were used to evaluate the mesenchymal characteristics of each cell line. Genes were matched to CCLE expression data based on HGNC symbols, extracting only columns corresponding to these EMT genes.

4.8.3. EMT Score Calculation

For each cell line, an EMT score was computed as the mean expression across all 200 EMT genes. Missing values were ignored in the calculation. This score provides a quantitative measure of the mesenchymal phenotype of each cell line.

4.8.4. Data Visualization

EMT scores were visualized using boxplots with the ggplot2 R package. Points were colored black and labeled with cell line names using the ggrepel package to avoid overlapping labels.

 doi:10.20944/preprints202603.2418.v1

Statistical comparisons between compact and loose spheroid groups were performed using an unpaired two-sided t-test (ggpubr package), with p-values reported on the plot.

4.8.5. Data Processing

All data processing, filtering, and analyses were performed in R version 4.4.4 (R Foundation for Statistical Computing, Vienna, Austria).

4.9. Statistical Analysis

Statistical analyses were performed to compare experimental groups based on initial cell seeding densities (1000, 2500, and 5000 cells per spheroid) in at least three independent experiments. All statistical analyses were conducted using GraphPad Prism version 10.02 (GraphPad Software). If the assumptions for parametric analysis were met, the statistical significance was analysed in one-way analysis of variance (ANOVA) to compare differences between groups. When only the assumption of normality was satisfied, Welch's ANOVA was applied to account for unequal variances. However, if both normality and homogeneity of variances were confirmed, the standard one-way ANOVA was performed. If the assumptions were not satisfied, the non-parametric Kruskal–Wallis test was used instead. The level of significance was set at *$p<0.05$, **$p<0.01$, ***$p<0.001$ and ****$p<0.0001$.

Supplementary Materials: The following supporting information can be downloaded at the website of this paper posted on Preprints.org.

Author Contributions: MMC contributed to the design of the experiments, conceived, data analysis, and writing of the manuscript. LM contributed to the performance of experiments, data analysis, and contributed to the writing of the manuscript. CE contributed to bioinformatics analysis and performed the immunohistochemistry and immunofluorescence experiments. BS contributed to the design of the experiments, supervision, and manuscript revision. CJ contributed to revising the manuscript and supervision. AJE contributed to revising the manuscript and supervision. JP contributed to the design of the experiments, writing and revising the manuscript, and supervision. All the authors read and approved the final manuscript.

Funding: This work was supported by two research grants (MMC: 2020.07439.BD; CE: 2022.11242.BD) funded by Fundação para a Ciência e Tecnologia (Portugal), by a research grant from the Breast Cancer Research Foundation (BCRF-24-048) to AJE, and by a research grant from Liga Portuguesa contra o Cancro (MMC).

Institutional Review Board Statement: Not applicable

Informed Consent Statement: Not applicable.

Data Availability Statement: All data generated or analysed during this study are included in this published article and its supplementary information files.

Acknowledgments: The authors acknowledge the technical support of the i3S Scientific Platforms - Advanced Light Microscopy, Bioimaging, and Histology and Electron Microscopy, and to the Porto Comprehensive Cancer Center (P.CCC) Raquel Seruca, for the institutional support.

Conflicts of Interest: AJE has unlicensed patents related to the use of antibodies as anti-cancer therapeutics and his spouse is an employee of Immunocore.

Appendix A

 doi:10.20944/preprints202603.2418.v1

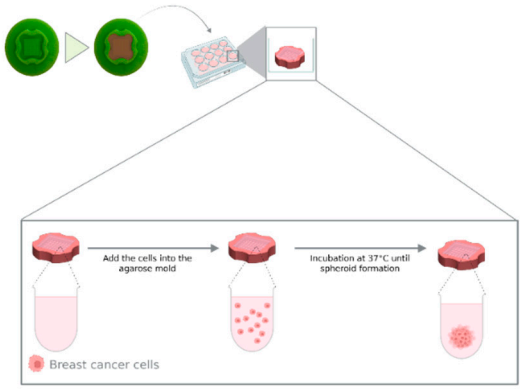

Figure A1. Graphic illustration of breast cancer tumour spheroids formation using the liquid overlay technique. Figure created with BioRender.com (accessed September, 2025).

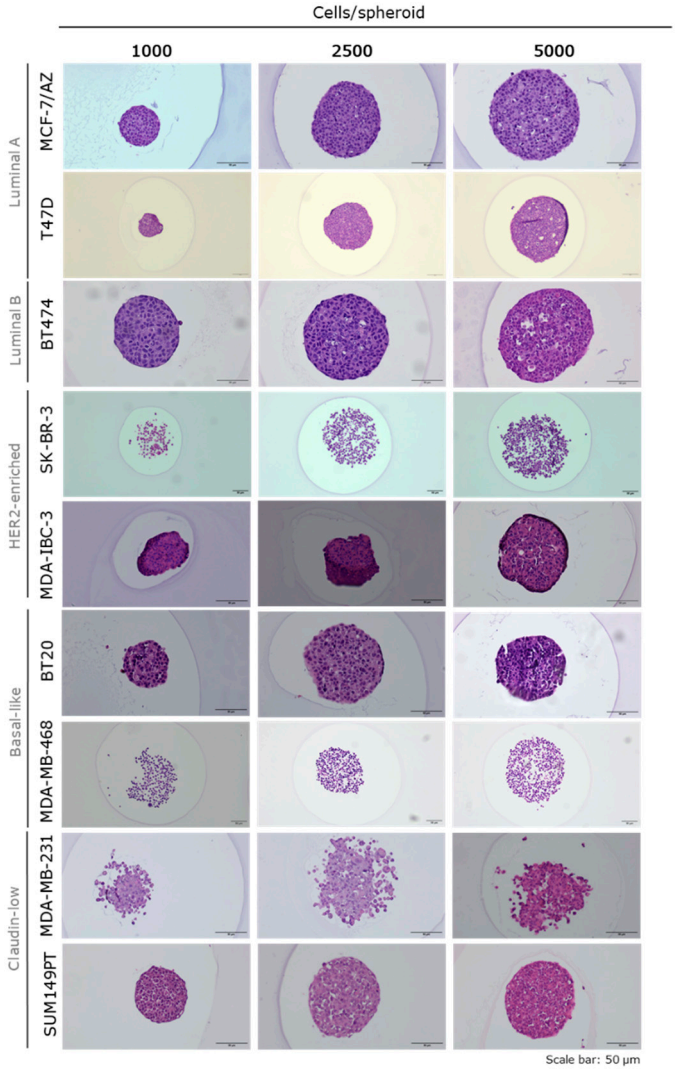

 doi:10.20944/preprints202603.2418.v1

Figure A2. Histological analysis by H&E staining of breast cancer spheroids after 48h grown in suspension in three cell densities. Scale bars represent 50 μm.

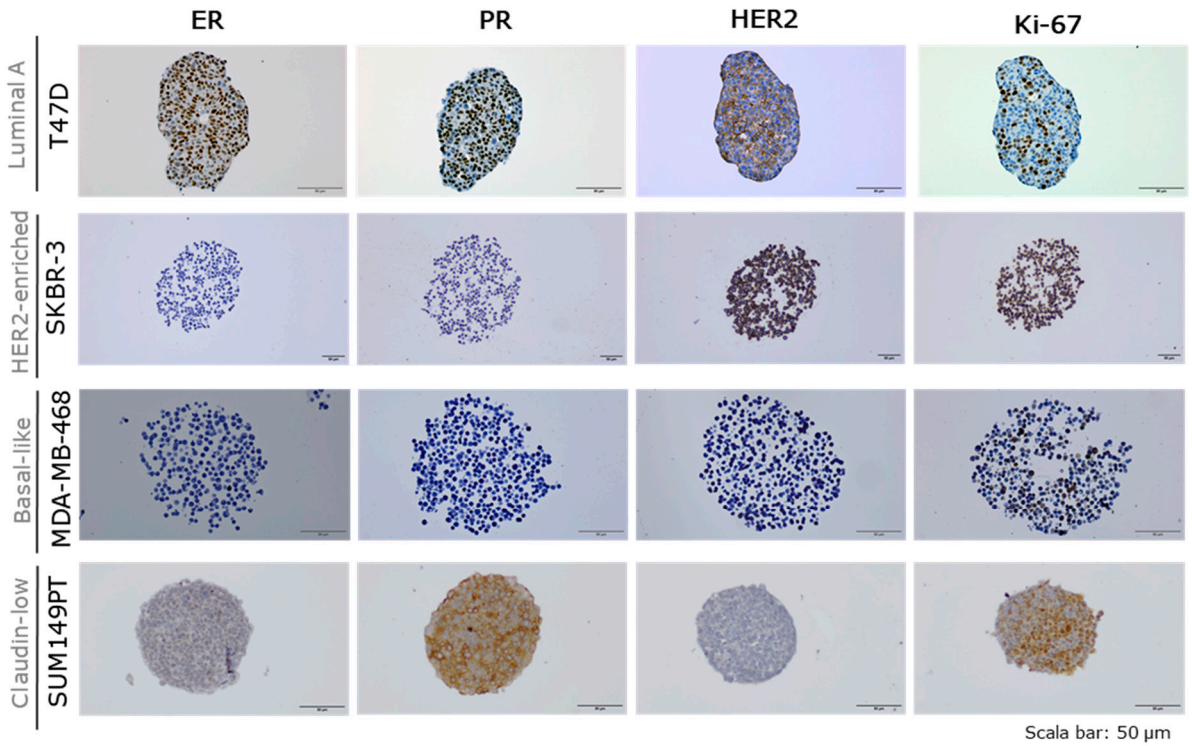

Figure A3. Representative images of breast cancer molecular subtypes (Luminal A-T47D, HER2-enriched–SKBR-3, Basal-like-MDA-MB-468, and Claudin-low–SUM149PT). Immunohistochemistry for the Hormonal receptors (ER-Estrogen; PR-Progesterone), human epidermal growth factor receptor 2 (HER-2) and Ki67 (proliferation marker) using breast cancer spheroids (2500 cells/spheroid). Scale bars represent 50 μm.

 doi:10.20944/preprints202603.2418.v1

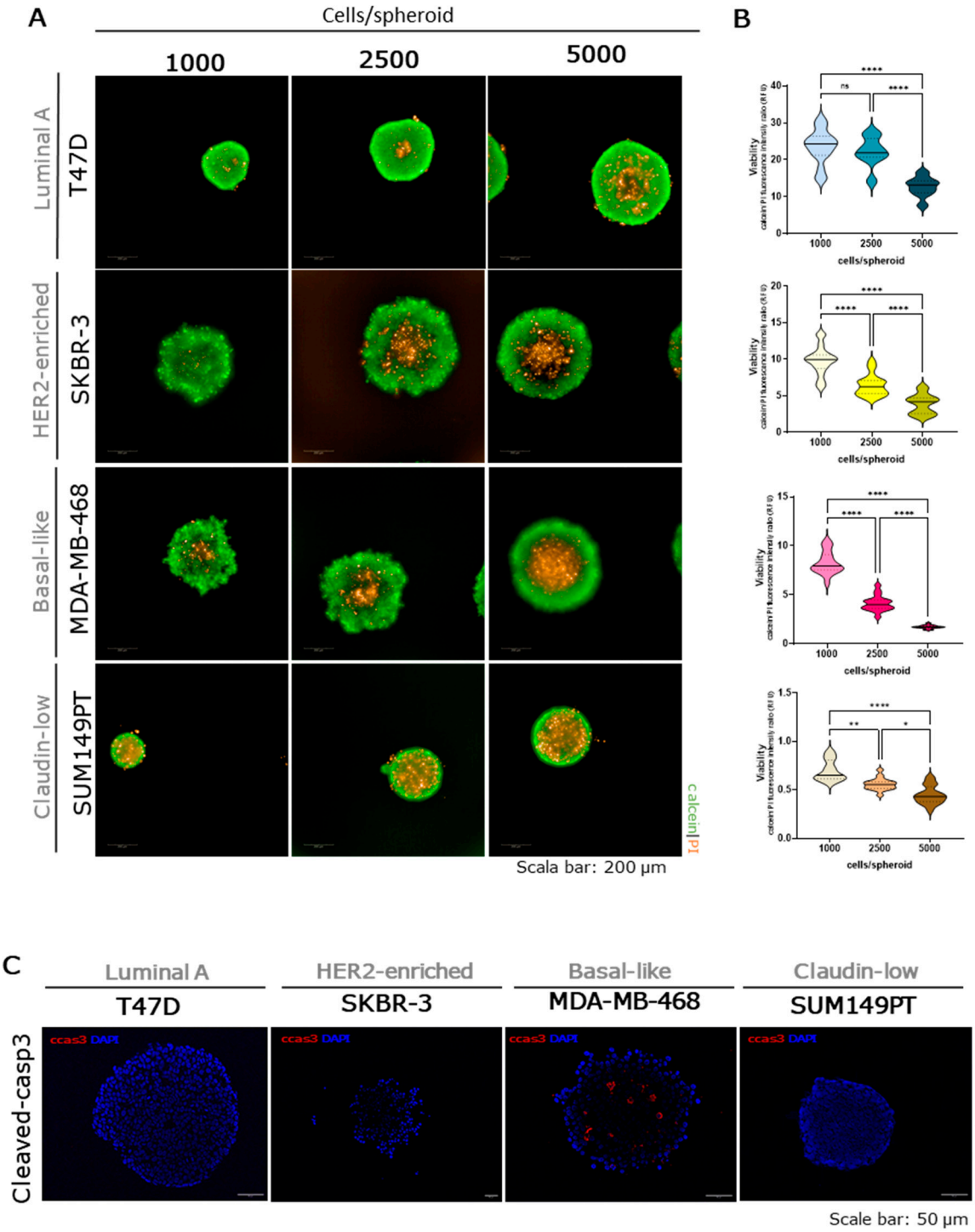

Figure A4. Evaluation of cell viability and cleaved-caspase 3 of breast cancer molecular subtype: Luminal A-T47D (blue), HER2-enriched–SKBR-3 (yellow), Basal-like-MDA-MB-468 (pink), and Claudin-low–SUM149PT (brown). Viability was evaluate using calcein/PI staining, where calcein (green) label live cells, and PI (red) the dead cells. Scale bars represent 200 µm [A]. Quantification of the fluorescent intensity (RFU -relative fluorescent units) of calcein and PI ratio using the Harmony high-content imaging and analysis software in three independent experiments [B]. Representative images of cleaved-caspase-3 (cCasp3, red) staining and nuclei counterstained with DAPI (blue) in the 2500 cells/spheroid after 48h in suspension. Scale bars represent 50 µm [C]. Data are shown as mean ± SD, and the level of significance was set at *p<0.05, **p<0.01, ***p<0.001 and ****p<0.0001.

Preprints.org (www.preprints.org) | NOT PEER-REVIEWED | Posted: 31 March 2026 doi:10.20944/preprints202603.2418.v1

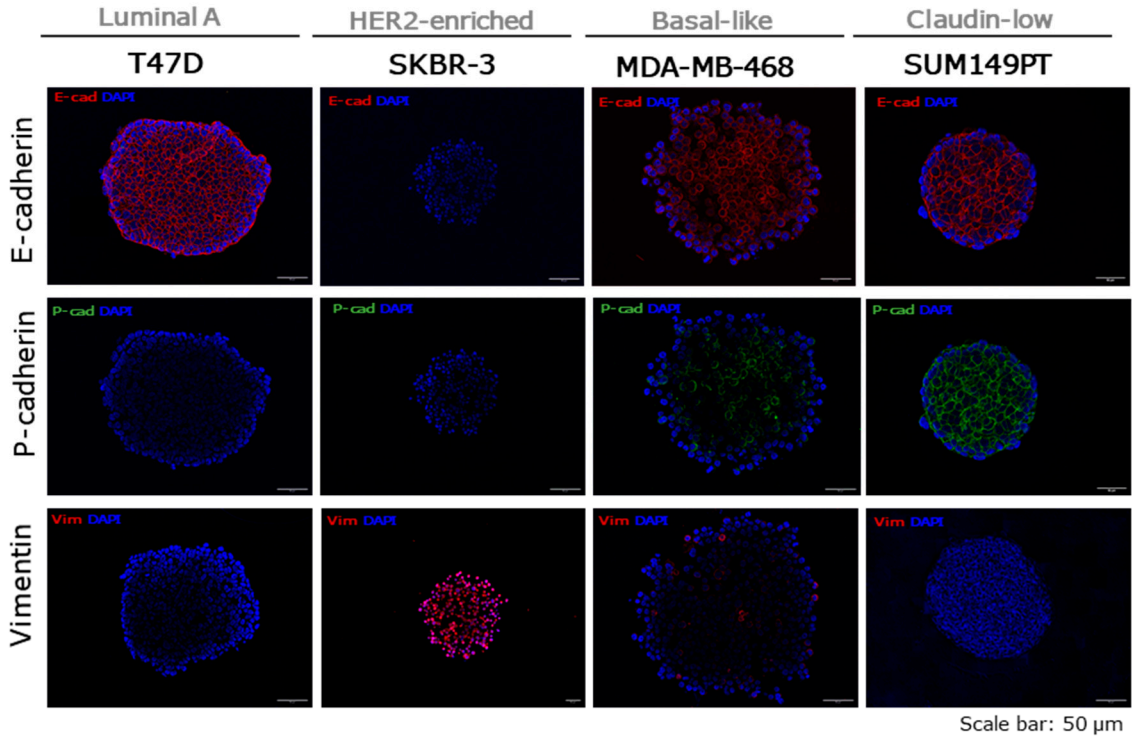

Figure A5. Representative images showing the expression of EMT markers of breast cancer molecular subtypes (Luminal A-T47D, HER2-enriched–SKBR-3, Basal-like-MDA-MB-468, and Claudin-low–SUM149PT). E-cadherin staining (red) was used as an epithelial marker, Vimentin staining (red) for mesenchymal marker, and E-cadherin (red) and P-cadherin (green) represent the hybrid EMT phenotype. All samples were counterstained with DAPI (blue). Scale bars represent 50 µm.

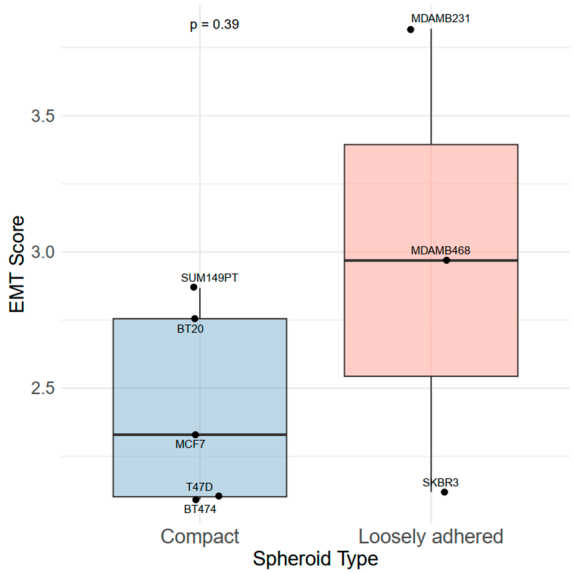

Figure A6. Boxplot showing the correlation between the EMT score and 3D spheroids' morphology: compact (MCF-7/AZ, T47D, BT474, BT-20, SUM149PT) or loose (SKBR-3, MDA-MB-468, MDA-MB-231). Graph and analysis performed in R software version 4.4.4.

Table A1. Antibodies dilutions used for protein detection by immunohistochemistry and immunofluorescence.

Immunohistochemistry				
Protein	**ER**	**PR**	**HER2**	**Ki67**

 doi:10.20944/preprints202603.2418.v1

Reference/Company	NCL-L-ER-6F11, Leica Biosystems	NCL-L-PGR, Leica Biosystems	Clone ab134182, Abcam	Clone MIB-1, Dako
Dilution	1:50	1:100	1:500	1:250
Immunofluorescence				
Protein	**cCasp3 (asp175) (D3E9)**	**E-cadherin**	**P-cadherin**	**Vimentin**
Reference/Company	9579S, Cell Signaling, USA	24E10, Cell Signaling, USA	Clone 56, BD Transduction, USA	D21H3, Cell Signaling, USA
Dilution	1:200	1:100	1:100	1:400

References

1. Bray F, Laversanne M, Sung H, Ferlay J, Siegel RL, Soerjomataram I, et al. Global cancer statistics 2022: GLOBOCAN estimates of incidence and mortality worldwide for 36 cancers in 185 countries. CA Cancer J Clin. 2024;74: 229–263. doi:10.3322/CAAC.21834;REQUESTEDJOURNAL:JOURNAL:15424863;WGROUP:STRING:PUBLICATION
2. Xiong X, Zheng LW, Ding Y, Chen YF, Cai YW, Wang LP, et al. Breast cancer: pathogenesis and treatments. Signal Transduct Target Ther. 2025;10: 1–33. doi:10.1038/S41392-024-02108-4;SUBJMETA
3. Perou CM, Sørile T, Eisen MB, Van De Rijn M, Jeffrey SS, Ress CA, et al. Molecular portraits of human breast tumours. Nature. 2000;406: 747–752. doi:10.1038/35021093;KWRD
4. Sørlie T, Perou CM, Tibshirani R, Aas T, Geisler S, Johnsen H, et al. Gene expression patterns of breast carcinomas distinguish tumor subclasses with clinical implications. Proc Natl Acad Sci U S A. 2001;98: 10869–10874. doi:10.1073/PNAS.191367098
5. Prat A, Perou CM. Deconstructing the molecular portraits of breast cancer. Mol Oncol. 2010;5: 5. doi:10.1016/J.MOLONC.2010.11.003
6. Carvalho E, Canberk S, Schmitt F, Vale N. Molecular Subtypes and Mechanisms of Breast Cancer: Precision Medicine Approaches for Targeted Therapies. Cancers 2025, Vol 17, Page 1102. 2025;17: 1102. doi:10.3390/CANCERS17071102
7. Lopez-Tarruella S, Del Monte-Millán M, Roche-Molina M, Jerez Y, Echavarria Diaz-Guardamino I, Herrero López B, et al. Correlation between breast cancer subtypes determined by immunohistochemistry and n-COUNTER PAM50 assay: a real-world study. Breast Cancer Res Treat. 2024;203: 163–172. doi:10.1007/S10549-023-07094-9/TABLES/4
8. Gutierrez C, Schiff R. HER2: Biology, Detection, and Clinical Implications. Arch Pathol Lab Med. 2011;135: 55–62. doi:10.5858/2010-0454-RAR.1
9. Schettini F, Prat A. Dissecting the biological heterogeneity of HER2-positive breast cancer. The Breast. 2021;59: 339–350. doi:10.1016/J.BREAST.2021.07.019
10. Romond EH, Perez EA, Bryant J, Suman VJ, Geyer CE, Davidson NE, et al. Trastuzumab plus adjuvant chemotherapy for operable HER2-positive breast cancer. N Engl J Med. 2005;353: 1673–1684. doi:10.1056/NEJMOA052122
11. Piccart-Gebhart MJ, Procter M, Leyland-Jones B, Goldhirsch A, Untch M, Smith I, et al. Trastuzumab after adjuvant chemotherapy in HER2-positive breast cancer. N Engl J Med. 2005;353: 1659–1672. doi:10.1056/NEJMOA052306
12. Podo F, Buydens LMC, Degani H, Hilhorst R, Klipp E, Gribbestad IS, et al. Triple-negative breast cancer: present challenges and new perspectives. Mol Oncol. 2010;4: 209–229. doi:10.1016/J.MOLONC.2010.04.006
13. Nielsen TO, Hsu FD, Jensen K, Cheang M, Karaca G, Hu Z, et al. Immunohistochemical and clinical characterization of the basal-like subtype of invasive breast carcinoma. Clin Cancer Res. 2004;10: 5367–5374. doi:10.1158/1078-0432.CCR-04-0220

 doi:10.20944/preprints202603.2418.v1

14. Prat A, Parker JS, Karginova O, Fan C, Livasy C, Herschkowitz JI, et al. Phenotypic and molecular characterization of the claudin-low intrinsic subtype of breast cancer. Breast Cancer Res 2010 125. 2010;12: R68-. doi:10.1186/BCR2635
15. Zanoni M, Cortesi M, Zamagni A, Arienti C, Pignatta S, Tesei A. Modeling neoplastic disease with spheroids and organoids. J Hematol Oncol. 2020;13: 1–15. doi:10.1186/S13045-020-00931-0/FIGURES/5
16. Boix-Montesinos P, Soriano-Teruel PM, Armiñán A, Orzáez M, Vicent MJ. The past, present, and future of breast cancer models for nanomedicine development. Adv Drug Deliv Rev. 2021;173: 306–330. doi:10.1016/j.addr.2021.03.018
17. Katt ME, Placone AL, Wong AD, Xu ZS, Searson PC. In vitro tumor models: Advantages, disadvantages, variables, and selecting the right platform. Front Bioeng Biotechnol. 2016;4. doi:10.3389/fbioe.2016.00012
18. Han SJ, Kwon S, Kim KS. Challenges of applying multicellular tumor spheroids in preclinical phase. Cancer Cell Int. 2021;21: 1–19. doi:10.1186/s12935-021-01853-8
19. Fennema E, Rivron N, Rouwkema J, van Blitterswijk C, De Boer J. Spheroid culture as a tool for creating 3D complex tissues. Trends Biotechnol. 2013;31: 108–115. doi:10.1016/J.TIBTECH.2012.12.003
20. Pinto B, Henriques AC, Silva PMA, Bousbaa H. Three-Dimensional Spheroids as In Vitro Preclinical Models for Cancer Research. Pharm 2020, Vol 12, Page 1186. 2020;12: 1186. doi:10.3390/PHARMACEUTICS12121186
21. Hirschhaeuser F, Menne H, Dittfeld C, West J, Mueller-Klieser W, Kunz-Schughart LA. Multicellular tumor spheroids: An underestimated tool is catching up again. J Biotechnol. 2010;148: 3–15. doi:10.1016/J.JBIOTEC.2010.01.012
22. Neve RM, Chin K, Fridlyand J, Yeh J, Baehner FL, Fevr T, et al. A collection of breast cancer cell lines for the study of functionally distinct cancer subtypes. Cancer Cell. 2006;10: 515–527. doi:10.1016/J.CCR.2006.10.008
23. Bauleth-Ramos T, Feijão T, Gonçalves A, Shahbazi MA, Liu Z, Barrias C, et al. Colorectal cancer triple co-culture spheroid model to assess the biocompatibility and anticancer properties of polymeric nanoparticles. J Control Release. 2020;323: 398–411. doi:10.1016/j.jconrel.2020.04.025
24. Domingues M, Leite Pereira C, Sarmento B, Castro F. Mimicking 3D breast tumor-stromal interactions to screen novel cancer therapeutics. Eur J Pharm Sci. 2023;190: 106560. doi:10.1016/j.ejps.2023.106560
25. Pastushenko I, Blanpain C. EMT Transition States during Tumor Progression and Metastasis. Trends Cell Biol. 2019;29: 212–226. doi:10.1016/J.TCB.2018.12.001
26. Lambert AW, Weinberg RA. Linking EMT programmes to normal and neoplastic epithelial stem cells. Nat Rev Cancer. 2021;21: 325–338. doi:10.1038/S41568-021-00332-6;SUBJMETA
27. Ribeiro AS, Paredes J. P-Cadherin Linking Breast Cancer Stem Cells and Invasion: A Promising Marker to Identify an "Intermediate/Metastable" EMT State. Front Oncol. 2015;4: 371. doi:10.3389/FONC.2014.00371
28. Jolly MK, Boareto M, Debeb BG, Aceto N, Farach-Carson MC, Woodward WA, et al. Inflammatory breast cancer: A model for investigating cluster-based dissemination. npj Breast Cancer. 2017;3: 1–8. doi:10.1038/S41523-017-0023-9;SUBJMETA
29. Canário R, Ribeiro AS, Morgado I, Peixoto A, Barbosa A, Santos C, et al. P-cadherin overexpression is associated with early transformation of the Fallopian tube epithelium and aggressiveness of tubo-ovarian high-grade serous carcinoma. Virchows Arch. 2025 [cited 8 Oct 2025]. doi:10.1007/S00428-025-04104-7
30. Jolly MK, Tripathi SC, Jia D, Mooney SM, Celiktas M, Hanash SM, et al. Stability of the hybrid epithelial/mesenchymal phenotype. Oncotarget. 2016;7: 27067–27084. doi:10.18632/ONCOTARGET.8166
31. Falkenberg N, Höfig I, Rosemann M, Szumielewski J, Richter S, Schorpp K, et al. Three-dimensional microtissues essentially contribute to preclinical validations of therapeutic targets in breast cancer. Cancer Med. 2016;5: 703–710. doi:10.1002/CAM4.630
32. T47D Cell Line Spheroid Generation and Characterization for HT Assays | Thermo Fisher Scientific - PT. [cited 6 Oct 2025]. Available: https://www.thermofisher.com/pt/en/home/references/protocols/cell-culture/3-d-cell-culture-protocol/t47d-cell-line-spheroid-generation.html?utm_source=chatgpt.com
33. Kenny PA, Lee GY, Myers CA, Neve RM, Semeiks JR, Spellman PT, et al. The morphologies of breast cancer cell lines in three-dimensional assays correlate with their profiles of gene expression. Mol Oncol. 2007;1: 84–96. doi:10.1016/j.molonc.2007.02.004

 doi:10.20944/preprints202603.2418.v1

34. Froehlich K, Haeger JD, Heger J, Pastuschek J, Photini SM, Yan Y, et al. Generation of Multicellular Breast Cancer Tumor Spheroids: Comparison of Different Protocols. J Mammary Gland Biol Neoplasia. 2016;21: 89–98. doi:10.1007/s10911-016-9359-2
35. Gong X, Lin C, Cheng J, Su J, Zhao H, Liu T, et al. Generation of Multicellular Tumor Spheroids with Microwell-Based Agarose Scaffolds for Drug Testing. PLoS One. 2015;10: e0130348. doi:10.1371/JOURNAL.PONE.0130348
36. Cavaco M, Fraga P, Valle J, Andreu D, Castanho MARB, Neves V. Development of breast cancer spheroids to evaluate cytotoxic response to an anticancer peptide. Pharmaceutics. 2021;13: 1863. doi:10.3390/PHARMACEUTICS13111863/S1
37. Lee GY, Kenny PA, Lee EH, Bissell MJ. Three-dimensional culture models of normal and malignant breast epithelial cells. Nat Methods. 2010;4: 359–365. doi:10.1038/nmeth1015.Three-dimensional
38. Hofmann S, Cohen-Harazi R, Maizels Y, Koman I. Patient-derived tumor spheroid cultures as a promising tool to assist personalized therapeutic decisions in breast cancer. Transl Cancer Res. 2022;11: 134–147. doi:10.21037/TCR-21-1577/COIF)
39. Koedoot E, Wolters L, Smid M, Stoilov P, Burger GA, Herpers B, et al. Differential reprogramming of breast cancer subtypes in 3D cultures and implications for sensitivity to targeted therapy. Sci Rep. 2021;11: 1–13. doi:10.1038/S41598-021-86664-7;SUBJMETA
40. Pickl M, Ries CH. Comparison of 3D and 2D tumor models reveals enhanced HER2 activation in 3D associated with an increased response to trastuzumab. Oncogene. 2009;28: 461–468. doi:10.1038/ONC.2008.394;KWRD
41. Krause S, Maffini M V., Soto AM, Sonnenschein C. The microenvironment determines the breast cancer cells' phenotype: Organization of MCF7 cells in 3D cultures. BMC Cancer. 2010;10: 1–13. doi:10.1186/1471-2407-10-263/FIGURES/8
42. Imamura Y, Mukohara T, Shimono Y, Funakoshi Y, Chayahara N, Toyoda M, et al. Comparison of 2D- and 3D-culture models as drug-testing platforms in breast cancer. Oncol Rep. 2015;33: 1837–1843. doi:10.3892/OR.2015.3767/HTML
43. Peirsman A, Blondeel E, Ahmed T, Anckaert J, Audenaert D, Boterberg T, et al. MISpheroID: a knowledgebase and transparency tool for minimum information in spheroid identity. Nat Methods. 2021;18: 1294. doi:10.1038/S41592-021-01291-4
44. Kirkegaard T, Hansen SK, Larsen SL, Reiter BE, Sørensen BS, Lykkesfeldt AE. T47D breast cancer cells switch from ER/HER to HER/c-Src signaling upon acquiring resistance to the antiestrogen fulvestrant. Cancer Lett. 2014;344: 90–100. doi:10.1016/J.CANLET.2013.10.014
45. Singh M, Mukundan S, Jaramillo M, Oesterreich S, Sant S. Three-dimensional breast cancer models mimic hallmarks of size-induced tumor progression. Cancer Res. 2016;76: 3732. doi:10.1158/0008-5472.CAN-15-2304
46. Park HJ, Helfman DM. Up-regulated fibronectin in 3D culture facilitates spreading of triple negative breast cancer cells on 2D through integrin β-5 and Src. Sci Rep. 2019;9: 1–14. doi:10.1038/S41598-019-56276-3;TECHMETA
47. Yersal O, Barutca S. Biological subtypes of breast cancer: Prognostic and therapeutic implications. World J Clin Oncol. 2014;5: 412–424. doi:10.5306/WJCO.V5.I3.412
48. Leung BM, Lesher-Perez SC, Matsuoka T, Moraes C, Takayama S. Media additives to promote spheroid circularity and compactness in hanging drop platform. Biomater Sci. 2015;3: 336–344. doi:10.1039/c4bm00319e
49. Zanoni M, Piccinini F, Arienti C, Zamagni A, Santi S, Polico R, et al. 3D tumor spheroid models for in vitro therapeutic screening: a systematic approach to enhance the biological relevance of data obtained. Sci Reports 2016 61. 2016;6: 19103-. doi:10.1038/srep19103
50. Mazloomi MA, Hamishehkar H, Jahanban Esfahlan R. SpheroidSync as edge cutting transfer strategy for uniform and robust MCF7 spheroids in 3D culture. Sci Reports 2025 151. 2025;15: 41237-. doi:10.1038/s41598-025-25202-1
51. Zhu S, Yin J, Lu X, Jiang D, Chen R, Cui K, et al. Influence of experimental variables on spheroid attributes. Sci Reports 2025 151. 2025;15: 9751-. doi:10.1038/s41598-025-92037-1

 doi:10.20944/preprints202603.2418.v1

52. Lerma E, Peiro G, Ramón T, Fernandez S, Martinez D, Pons C, et al. Immunohistochemical heterogeneity of breast carcinomas negative for estrogen receptors, progesterone receptors and Her2/neu (basal-like breast carcinomas). Mod Pathol. 2007;20: 1200–1207. doi:10.1038/MODPATHOL.3800961
53. Hollestelle A, Elstrodt F, Timmermans M, Sieuwerts AM, Klijn JGM, Foekens JA, et al. Four human breast cancer cell lines with biallelic inactivating α-catenin gene mutations. Breast Cancer Res Treat. 2010;122: 125–133. doi:10.1007/S10549-009-0545-4/TABLES/2
54. Mangani S, Koutsakis C, Koletsis NE, Piperigkou Z, Franchi M, Götte M, et al. Spheroid-Based 3D Models to Decode Cell Function and Matrix Effectors in Breast Cancer. Cancers 2025, Vol 17,. 2025;17. doi:10.3390/CANCERS17213512
55. Huang Z, Yu P, Tang J. Characterization of Triple-Negative Breast Cancer MDA-MB-231 Cell Spheroid Model. Onco Targets Ther. 2020;13: 5395–5405. doi:10.2147/OTT.S249756
56. Arnaldi P, Zotti VD, Bellese G, Gagliani MC, Orecchia P, Castagnola P, et al. 3D Breast Cancer Spheroids Reveal Architecture-Dependent HER2 Expression and Signaling. Biol 2025, Vol 14,. 2025;14: 1654. doi:10.3390/BIOLOGY14121654
57. Piwocka O, Sterzyńska K, Malińska A, Suchorska WM, Kulcenty K. Development of tetraculture spheroids as a versatile 3D model for personalized breast cancer research. Sci Rep. 2025;15: 1–14. doi:10.1038/S41598-025-12556-9;SUBJMETA
58. Ahvaraki A, Gheytanchi E, Behroodi E, Latifi H, Vakhshiteh F, Bagheri Z, et al. Advanced co-culture 3D breast cancer model to study cell death and nanodrug sensitivity of tumor spheroids. Biochem Eng J. 2024;209: 109400. doi:10.1016/J.BEJ.2024.109400
59. Diosdi A, Piccinini F, Boroczky T, Dobra G, Castellani G, Buzas K, et al. Single-cell light-sheet fluorescence 3D images of tumour-stroma spheroid multicultures. Sci Data 2025 121. 2025;12: 492-. doi:10.1038/s41597-025-04832-0
60. Saraiva DP, Matias AT, Braga S, Jacinto A, Cabral MG. Establishment of a 3D Co-culture With MDA-MB-231 Breast Cancer Cell Line and Patient-Derived Immune Cells for Application in the Development of Immunotherapies. Front Oncol. 2020;10: 561826. doi:10.3389/FONC.2020.01543/BIBTEX
61. Ortiz E, Thway KH, Ortiz-Soto G, Yao P, Kelber JA. Hetero-multicellular stromal cells incorporate into scaffold-free 3D cultures of epithelial cancer cells to drive invasion. bioRxiv. 2025; 2025.01.21.634082. doi:10.1101/2025.01.21.634082
62. Chen G, Liu W, Yan B, Chen G, Liu W, Yan B. Breast Cancer MCF-7 Cell Spheroid Culture for Drug Discovery and Development. J Cancer Ther. 2022;13: 117–130. doi:10.4236/JCT.2022.133009
63. Coelho LL, Vianna MM, da Silva DM, Gonzaga BM de S, Ferreira RR, Monteiro AC, et al. Spheroid Model of Mammary Tumor Cells: Epithelial–Mesenchymal Transition and Doxorubicin Response. Biol 2024, Vol 13,. 2024;13. doi:10.3390/BIOLOGY13070463
64. Lin YN, Nasir A, Camacho S, Berry DL, Schmidt MO, Pearson GW, et al. Monitoring cancer cell invasion and t-cell cytotoxicity in 3d culture. J Vis Exp. 2020;2020: 1–19. doi:10.3791/61392
65. Silveira MJ, Martins C, Cardoso AP, Ankone MJK, Blyth RRR, Oliveira MJ, et al. Immunostimulatory effects of IL-12 targeted pH-responsive nanoparticles in macrophage-enriched 3D immuno-spheroids in vitro model. Drug Deliv Transl Res. 2025; 1–20. doi:10.1007/S13346-025-01896-8/FIGURES/6
66. Kessel S, Cribbes S, Déry O, Kuksin D, Sincoff E, Qiu J, et al. High-Throughput 3D Tumor Spheroid Screening Method for Cancer Drug Discovery Using Celigo Image Cytometry. SLAS Technol. 2017;22: 454–465. doi:10.1177/2211068216652846